Asymmetric interface temperature during vapor bubble growth

A. Diana,[1,2,a)] M. Castillo,[2] T. Steinberg,[2] and D. Brutin[1,b)]
[1]*Aix-Marseille University, IUSTI UMR 7343 CNRS, 13013 Marseille, France*
[2]*School of Chemistry, Physics and Mechanical Engineering, Queensland University of Technology, Brisbane, QLD 4001, Australia*

(Received 18 April 2013; accepted 25 June 2013; published online 15 July 2013)

We investigate the nucleation, growth, and detachment of single vapor bubbles at the interface microscale. Shear flow is used to investigate pool and convective boiling situations using visible and infrared visualizations. We determine a threshold Reynolds number for the onset of asymmetric interfacial temperatures. Below this threshold, bubble growth is geometrically and thermally symmetric, while above, bubbles no longer grow thermally symmetrically. This is explained by the dominance of convective heat transfer removal over viscous effects at the bubble interface. We experimentally demonstrate asymmetric interfacial temperature profiles that should be taken into account for future bubble growth modeling. © *2013 AIP Publishing LLC*. [http://dx.doi.org/10.1063/1.4813561]

Convective boiling is a very efficient heat transfer method due to the latent heat transferred during the phase change. It is encountered in many engineering fields such as energy conversion, environmental applications, food and chemical processes as well as in space and aeronautic applications. However, nucleation and heat transfer issues related to the boiling phenomenon can be problematic in several other areas like chemistry during electrolysis when nucleation appears on the electrode. During fast charging, nucleation degrades the substrate quality and subsequently the transfer of electrons. This wide range of applications makes nucleation/boiling an important subject, especially in a world context of energy savings and heat transfer enhancement. For that purpose, a better comprehension of these phenomena at the bubble scale is needed to understand the heat transfer mechanisms and make more accurate predictions and improvements. Studies at the microscale, especially at the scale of vapor bubbles, are limited in literature. Nucleation, growth, and detachment of single vapor bubbles have been studied for pool and convective situations and are essential for theoretical and numerical modeling. Current models and correlations show good agreement with the bubbles' dynamic geometry.[1,2] However, microscale heat transfer studies at the liquid-vapor interface are still missing. There are only a few studies focusing on the triple line heat transfer,[3] which is the location where most of the heat transfer occurs.

All models published in literature assume an isothermal vapor bubble temperature in which the vapor remains at the saturation temperature corresponding to the pressure inside the bubble.[4,5] In the situation of pool boiling, this assumption can be valid; however, in the situation of convective boiling, convection of the liquid surrounding the vapor bubble could induce a temperature gradient along the bubble interface. What is this temperature gradient?

In this letter, we investigate the local growth of a single vapor bubble in shear flow to model different boiling situations. Our measurements and observations are at the bubble scale and cover both hydrodynamics and heat transfer. The bubble growth dynamics are well-described by existing models, but nothing exists regarding the bubble interfacial temperatures. Despite a perfectly symmetric growth, we observed an asymmetric thermal growth of the liquid-vapor interface as soon as the convective forces dominated over the viscous forces.

This study was performed using a fluid loop situated inside a confinement box. It was thermally regulated using Peltier elements to a temperature close to the fluids saturation point, typically 2 °C below saturation. The fluid, stored in 25 ml-syringes, was injected using a syringe pump into the test cell, which required a small amount of power to induce boiling. Barthes *et al.*[6] showed that the mirage effect produces a significant error in locating the interface when generating a vapor bubble on a downward facing element. Kenning *et al.*[7] showed several limitations for visualizing boiling with video measurements through the liquid. Consequently, we use a Hele-Shaw flow chamber heated at its upper face. The geometry of the cell was chosen to avoid three-dimensional effects and optical aberrations due to high thermal gradients in the thermal boundary layer.

We control the parameters related to the heating of the liquid and the fluid velocity; more specifically, we control liquid inlet temperature in the cell, mass flow rate, and heat flux at the substrate level. The cell is made out of polycarbonate with two opposite side faces made of Lexan and CaF_2. The CaF_2 face is transparent to infrared (IR) radiation between 3 and 5 μm and was treated to obtain a total transmissivity of 90%. Heating is ensured by an Inconel thin film (10 mm x 1 mm) that is powered electrically. The thin film is 100 μm thick with an electrical resistance of 1.0 Ω and has a 50 μm triangular hole to create a unique artificial nucleation site where single vapor bubbles nucleate. More details regarding the test cell can be found in Serret *et al.*[8]

All experiments are carried out according to the same experimental procedure. At a constant mass flow rate and heat flux, we continuously acquire visible and infrared images. Visual images are acquired through the Lexan face with an EOS 7 HD camera at 50 frames/s and infrared images are acquired through the CaF_2 face with an FLIR SC6000 infrared camera at the same frequency. Experiments

a)Electronic mail: antoine.diana@polytech.univ-mrs.fr
b)Electronic mail: david.brutin@univ-amu.fr

are carried out using HFE-7000 from 3 M because of its physical properties such as being odorless, nonflammable, non-explosive, semitransparent in the infrared wavelengths, and having low phase change enthalpy and low boiling temperature. The HFE-7000 density is $1400\,kg/m^3$, its saturation temperature at 1 bar is $T_{sat} = 34\,^{\circ}C$, its specific heat is $C_p = 142\,kJ \cdot kg^{-1}$, and its thermal conductivity is $\lambda = 0.075\,W \cdot m^{-1} \cdot K^{-1}$. HFE-7000 emissivity for a liquid thickness of 0.5 mm (half the gap between the two plates) is $\epsilon = 0.52$.

From the infrared and visible visualizations, we extract all the parameters regarding the bubble nucleation, growth, and detachment cycle. One originality of this work is that all data acquisitions are performed simultaneously using the cameras. This procedure allows us to provide accurate geometrical information and local interface temperatures. The infrared camera calibration is performed by comparing the fluid inlet temperature, given by a thermocouple placed in the fluid loop, and the camera temperature. The temperature difference between these two values is less than 0.1 °C. For several heat fluxes and shear rates, bubble geometrical evolution is plotted in Fig. 1. The bubble growth rate is determined either through visible data or using a correlation based on infrared visualization. From the visible data, the evolution of the bubble radius is obtained by measuring it directly on the pictures.

The results obtained from these two methods agree well with the results published by Duhar *et al.*[9] The radius follows a power law evolution (Eq. (1)) where k is a constant, Ja is the Jacob number defined by Eq. (2), and α is the thermal diffusivity defined by Eq. (3). The wall temperature (T_w) is the nucleation site temperature obtained using infrared visualization

$$R(t) = kJa\sqrt{\alpha t}, \tag{1}$$

$$Ja = \frac{\varrho_L Cp_L (T_w - T_{sat})}{\varrho_V L_V}, \tag{2}$$

$$\alpha = \frac{\lambda}{\varrho_L Cp_L}. \tag{3}$$

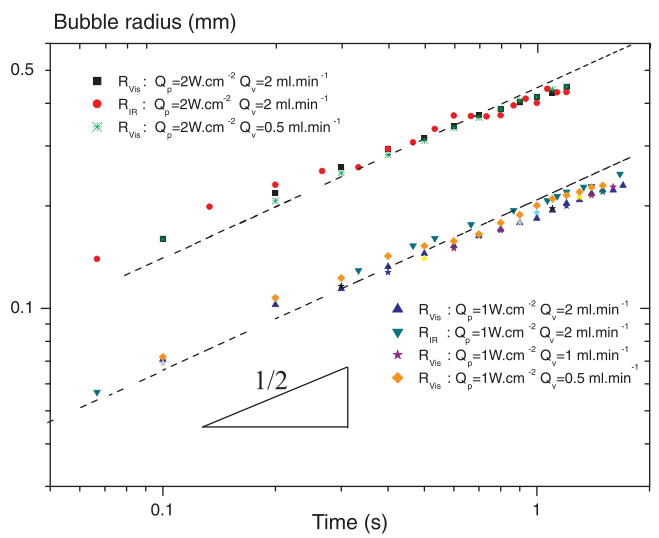

FIG. 1. Bubble radius evolution using visible and infrared techniques for several heat fluxes and shear flows. Power law evolutions are evidenced with a 1/2 slope, which is in agreement with classical literature observations (log-log scale). This validates our geometrical observations.

The value of k is not very sensitive to the fluid velocity or heat flux for this study (k = 0.3 for all the tested heat fluxes and flow rates). The experimental value of k can be compared to other models in literature based on different assumptions. Cooper and Lloyd[10] assumed that the bubble growth is mainly due to the evaporation of the micro layer below the bubble base. They found a value of $k = 2.5Pr^{-1/2}$, where Pr is the Prandtl number. For HFE-7000, k = 0.89. Other models based on evaporation on the whole bubble surface[11] lead to a value of k ranging between 1 and 2. The experimental value obtained in this study tends to show that the bubble growth is not only driven by the evaporation at the triple line but possibly also along the liquid-vapor interface when the bubble grows in shear flow.

In regards to the bubble interface temperature homogeneity, we observe the liquid-vapor interface dynamic during bubble nucleation until its detachment using infrared visualization. Figure 2 shows an image of a vapor bubble just before its detachment from the nucleation site. The shear flow is from right to left. The heating element is at the top of the test cell. The exact position of the interface is underlined (dotted line) in an image obtained from the visible light camera. Thanks to the calibration, the infrared image enables us to determine the temperature field around the vapor bubble in the liquid. Because the radiative heat flux arriving at the infrared camera detector comes from the heated liquid, the data analysis is performed only in the liquid part and at the bubble interface. Assuming a curved bubble interface in between the two Hele-Shaw plates, the temperature coming from the interface is the one coming from the liquid side. No quantitative data analysis is performed using temperature coming from the inside of the bubble because that region is vapor and has undetermined emissivity. From a geometrical point of view, the vapor bubble remains perfectly axisymmetric independent of the flow rate and heat flux. Because the mass flow rates are relatively low, the bubble shape remains symmetric on both sides of the bubble apex

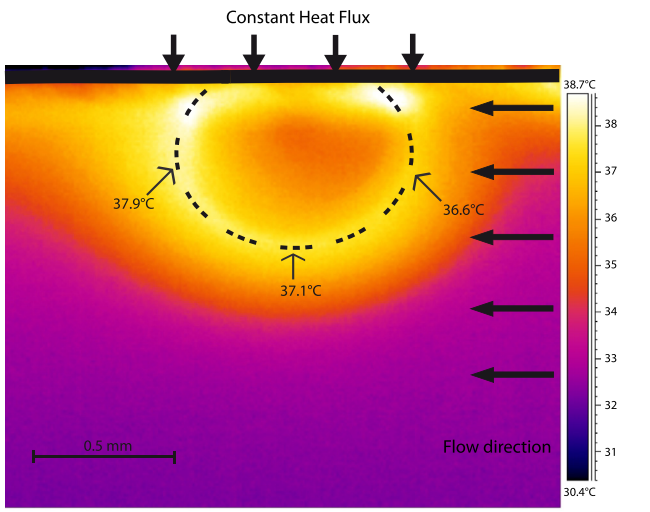

FIG. 2. Infrared visualization of the bubble prior to departure from the artificial nucleation site where a constant heat flux is applied. The liquid-vapor interface (dotted line) is precisely located using the visible light camera. A symmetric bubble from a geometric point of view is observed; on the other hand, an asymmetric bubble is observed in terms of interfacial temperature, with lower interfacial temperature facing the flow.

upstream and downstream of the flow. Fig. 2 shows that just before bubble detachment, an asymmetric bubble interface temperature exists for specific conditions; however, it is possible that such asymmetry may not exist for all shear flows and heat fluxes. Two heat transfer mechanisms are involved in convective boiling: viscous and convective forces. To evaluate the effects of both on the bubble interface temperature, we analyzed interfacial temperatures under a constant heat flux for different shear flows. The competition between the two forces is compared using the Reynolds number, which is based on the bubble diameter instead of the hydraulic diameter in order to be related to the bubble itself without the test cell influence. Based on this definition of the Reynolds number, our transitional Reynolds number is not dependent on the experimental configuration. Such a dimensionless value is changed by varying the shear flow. For the situations of Fig. 3, the Reynolds number is varied between 0.58 and 2.34, and the bubble interface temperatures are plotted as a function of the bubble curvilinear abscissa, where the origin corresponds to the bubble apex. While literature has only shown constant bubble interface temperatures far from the triple line, with Fig. 3, we provide experimental evidence that this interfacial temperature is not constant and not always symmetric depending on the shear flow. For Reynolds numbers less than or equal to 0.82, a symmetric bubble interfacial temperature exists on the bubble from its nucleation to its detachment (Figs. 3(a) and 3(b) in which 5 temperature profiles at different stages of the growth are provided). For Reynolds numbers greater than or equal to 1.17 (Figs. 3(c) and 3(d)), the bubble interfacial temperature is always asymmetric from its nucleation to its detachment. These temperature differences along the bubble interface cannot be neglected as they can reach values of 1.5 °C along

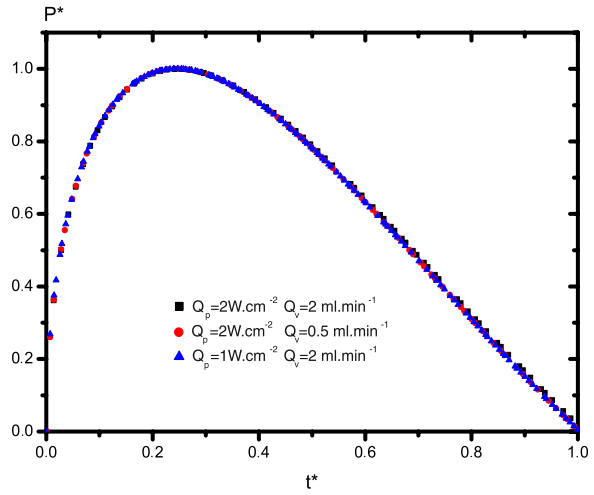

FIG. 4. Power required by a bubble to grow from nucleation to detachment. There is similar behavior regardless of the flow rates and heat fluxes used. The maximum power absorbed by the bubble occurs at 25% of the bubble lifetime. This time corresponds to the onset of thermal asymmetry of the bubble interface $P^* = \frac{P}{P_{max}}$ and $t^* = \frac{t}{t_f}$.

an interface of 0.8 mm *in situ*ations like those shown in Fig. 3(d). The temperature gradient is here sufficient enough to initiate capillary convection in the liquid. In the situation of Figs. 3(c) and 3(d), the bubble interface temperature starts to become dissymetric after t = 0.3 s. This can be explained by the bubble size. Before that critical time, the bubble size is only a few hundred micrometers. At some point, the bubble radius reaches a critical size where the convective forces overcome the viscous forces and the heat transfer coefficient around the bubble is no longer the same upstream and downstream of the flow. Consequently, the bubble interface temperature is no more symmetric. The degree of asymmetry is

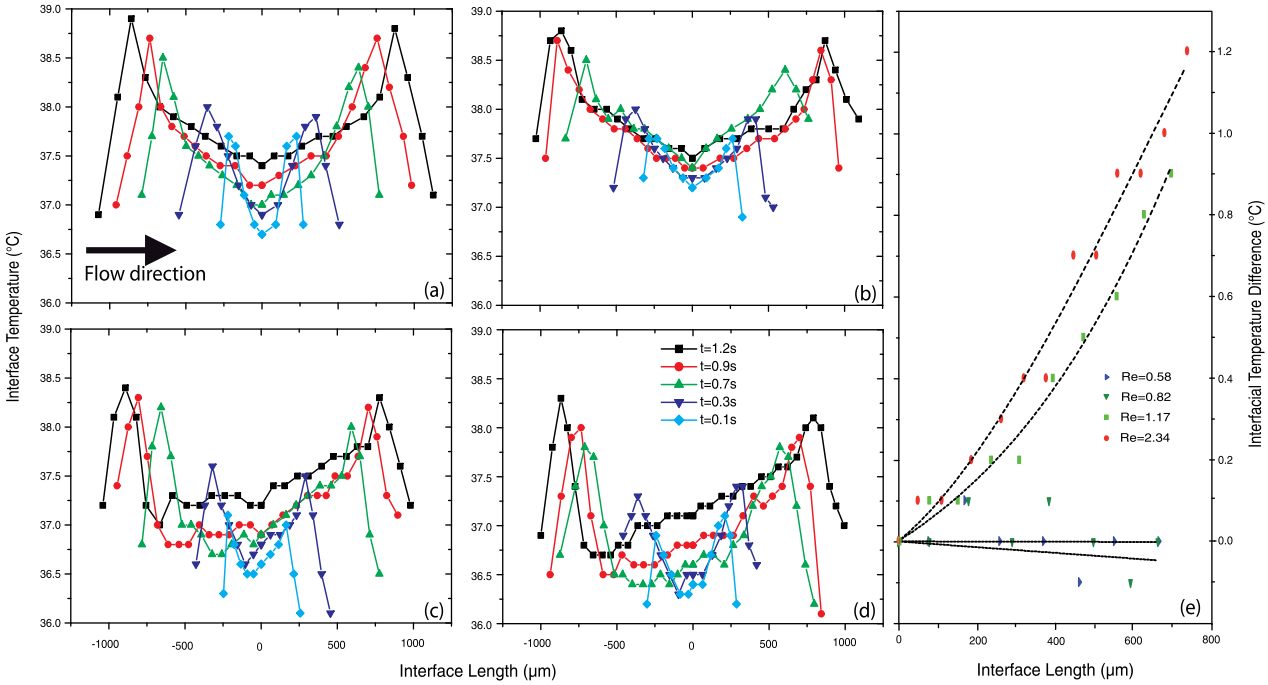

FIG. 3. Temperature along the bubble liquid-vapor interface for different flow rates at different stages of bubble growth. Asymmetric bubble growth occurs for Re > 1, where the temperature along the interface varies for upstream and downstream positions in regards to flow. For Re < 1, the bubble remains thermally symmetric. $Q_p = 2\,\mathrm{W}\cdot\mathrm{cm}^{-2}$; (a) Re = 0.58, (b) Re = 0.82, (c) Re = 1.17, and (d) Re = 2.34. The degree of asymmetry is quantified on the right side Figure 3(e) where the temperatures on each side of the bubble are compared at t = 1.2 s.

TABLE I. Dimensionless numbers characterizing the flow and the thermal, viscous and capillary effects. Bo_s, the static bond number is 0.94 [$Re_D = \frac{\rho VD}{\mu}$, $Ca = \frac{\mu V}{\sigma}$, $We = \frac{\rho V^2 L}{\sigma}$, $Ma = -\frac{d\sigma}{dT}\frac{1}{\mu\alpha}L\Delta T$, $Ra = \frac{g\beta}{\nu\alpha}(T_w - T_\infty)L^3$, $Bo_d = \frac{Ra}{Ma}$, $Bo_s = \frac{D}{\sqrt{\frac{\sigma}{\rho g}}}$].

Q_v	Re	Ca	We	Ma	Ra	Bo_d
0.5	0.58	1.5×10^{-5}	1.9×10^{-5}	13 754	7331	0.53
0.7	0.82	2.1×10^{-5}	3.8×10^{-5}	12 608	7494	0.59
1	1.17	3×10^{-5}	7.8×10^{-5}	10 888	7331	0.67
2	2.34	6×10^{-5}	31×10^{-5}	9169	7494	0.81

quantified in Fig. 3(e) by comparing the temperature between each side of the interface. It shows no difference, thus, a symmetry, when the Reynolds number is below the critical value and an increasing temperature difference when over the critical value of the Reynolds, demonstrating an asymmetric temperature profile. That critical stage of the bubble growth corresponds to the maximal heat flux absorbed by the bubble. This is confirmed by Fig. 4, where we plot the power required by the bubble to grow based on its geometrically measured evolution (based on Fig. 1), which is mathematically displayed by Eq. (4)

$$P(t) = \varrho_v L_v \frac{dV}{dt}. \tag{4}$$

In Figure 4, three power evolutions are plotted for different experimental conditions. All three curves show the same dimensionless evolution. The power absorbed by the bubble reaches a maximum at $t^* = 0.25$ regardless of inlet conditions.

The comparison of the dimensionless number characterizing vapor bubble growth in shear flow is presented in Table I. The calculation of these dimensionless numbers validates the hypothesis made previously. It shows for all situations we have $Ma > Ra$, which proves that surface tension is slightly dominant over the effect of gravity. Because the capillary number is slightly greater than 10^{-5}, inertial effects and the viscous forces contribute to heat transfer and the instabilities around the bubble. Based on these values and our experimental observations, we conclude that vapor bubble nucleation, growth, and detachment are driven by the three mechanisms: gravity forces, viscous forces, and surface tension forces. Our transition to thermal asymmetry is observed at a Reynolds number between 0.82 and 1.17. So above these values, the inertial forces are dominant in front of the viscous ones. The heat removal is then more important by heat convection than by viscous dissipation. Below these values, the viscous forces are dominating the inertial ones. The bubble interface temperature is there more uniform due to the low heat transfer removal by forced external convection. The assumption of constant interfacial temperature is no longer justified. To obtain accurate results, the bubble surface temperature variation has to be taken into account.

Our experimental results show that the bubble interface temperature far from the triple line is not constant. Furthermore, we demonstrate that in a situation of pool boiling, bubble growth is perfectly symmetric both geometrically and thermally. However, for convective boiling, a critical bubble Reynolds number exists to distinguish two thermal situations. Below that threshold, the bubble grows thermally symmetrically, while above, the bubble interface temperature exhibits a dissymmetric profile along the interface. We show that this threshold corresponds to the time in which convective forces become dominant over viscous forces. In that regime, the convective heat transfer facing the flow is no more the same as the heat transfer behind the bubble. Consequently, in most of the situations encountered in mechanical and chemical engineering applications, the constant interface temperature assumption is untrue and should be updated by taking into account the local heat transfer removal effect. The experimental interface temperature gradient observed confirms the existence of thermo-capillary convection because a strong gradient of surface tension exists.

We thank the French National Research Agency for their financial support through the ANR NanoSurf (ANR-09-BLAN-0093-03) as well as the European Space Agency for their support through the MAMBO Grant. We are also very grateful to J. Barber, for her contribution to the preliminary experiments.

[1]M. G. Cooper, K. Mori, and C. R. Stone, Int. J. Heat Mass Transfer **26**, 1489–1501 (1983).
[2]N. Zuber, Int. J. Heat Mass Transfer **2**, 83–98 (1961).
[3]N. Schweitzer and P. Stephan, Multiphase Sci. Technol. **21**, 329–350 (2009).
[4]P. Genske and K. Stephan, Int. J. Therm. Sci. **45**, 299–309 (2006).
[5]G. Son and V. K. Dhir, Int. J. Heat Mass Transfer **51**, 2566–2582 (2008).
[6]M. Barthes, C. Reynard, R. Santini, and L. Tadrist, in Proceedings of STAIF, Albuquerque, 2004.
[7]D. Wen, Y. Yan, and D. Kenning, Appl. Therm. Eng. **24**, 1207–1223 (2004).
[8]D. Serret, D. Brutin, O. Rahli, and L. Tadrist, Microgravity Sci. Technol. **22**, 377–385 (2010).
[9]G. Duhar, G. Riboux, and C. Colin, Heat Mass Transfer **45**, 847–855 (2009).
[10]M. G. Cooper and A. J. P. Lloyd, Int. J. Heat Mass Transfer **12**, 895–913 (1969).
[11]B. B. Mikic, W. M. Roshenow, and P. Griffith, Int. J. Heat Mass Transfer **13**, 657–666 (1970).